Revista Mexicana de Física **43**, *No. 2 (1997) 167–174*

Tomographic phase-distribution edge enhancement with differences of parallel projections: a proposal

G. RODRÍGUEZ-ZURITA AND R. PASTRANA-SÁNCHEZ*
Benemérita Universidad Autónoma de Puebla
Facultad de Ciencias Físico-Matemáticas
Apartado postal 1152, 72000 Puebla, Pue., México

Recibido el 11 de julio de 1996; aceptado el 16 de enero de 1997

ABSTRACT. The possibility for a method to enhance two-dimensional refractive-index distributions by using difference of parallel projections and tomographic retrieval techniques is discussed and some examples are given.

RESUMEN. Se plantea la posibilidad de un método capaz de proporcionar distribuciones bidimensionales de índice de refracción con sus bordes realzados y basados en diferencias de proyecciones paralelas junto con técnicas de reconstrucción tomográficas. Se presentan también algunos ejemplos numéricos.

PACS: 42.30.W; 42.40.K; 06.20; 42.65.H

1. INTRODUCCIÓN

Some improvements in wave-front transient double-exposure with photorefractive crystals with impact in the field of interferometric inspection of an object or a process have been recently reported [1, 2]. The potential of transient double-exposure in this field has been recognized early in the study of differential aspects such as the velocity in fluids [3], or the measurement of directional derivatives of rigid phase distributions by inducing object changes like rigid translations [4]. But induced changes as rotations seem to have received little attention, if any, in spite of its direct connection with optical tomography. In optical tomography a refractive-index distribution $f(x, y)$ within a region is to be found on the basis of emerging wave-fronts after they propagate through the object at known angles of projection ϕ. At the detection stage, interferometric techniques have to be incorporated to allow phase extraction [5] and reconstruction of the phase distribution can be carried out with appropriate algorithms [6].

Along this letter, a novel relation between transient storage and optical tomography is proposed on the basis of transient holographic double-exposure wave-front reconstruction of two wave fronts with phase distributions $\varphi(p, \phi)$ and $\varphi(p, \phi + \Delta\phi)$ emerging from a rotating object (each front recorded at slightly different projecting angles ϕ and $\phi + \Delta\phi$,

*INAOE graduate student and scholarship from CONACyT

p being the projection coordinate). Both waves can produce a transient interference pattern carrying the phase difference information $\Delta\varphi = \varphi(p, \phi + \Delta\phi) - \varphi(p, \phi)$. This information would eventually retrieve the refractive-index distribution $f(x, y)$ after two steps: first, an integration process leading to φ, and later, by employing the proper tomographic reconstruction algorithm (backprojection within the regime of refraction less limit, for example) $f(x, y)$ could be reconstructed. A tomographic retrieve method following these two steps is described in Ref. 7, where directional derivatives were the basis of the data rather than angular derivatives. However, as a property of the method proposed in this communication, we emphasize its possibility to take direct advantage of the attainable angular difference information to gain knowledge of $f(x, y)$ without the need of an intermediate integration process.

In the following, the basis for extracting differential information of a refractive-index distribution by means of differences of parallel projections is presented and some examples (both analytical and numerical) are also given.

2. ANGULAR DERIVATIVE OF OBJECTS AND THEIR PARALLEL PROJECTIONS

Consider a rigid refractive-index distributions $f(x, y)$ rotating at a constant angular velocity. At a given position, when the phase object is trans-illuminated with a bundle of parallel rays traveling along some fixed direction, the optical pathlength of a light ray is the path integral [8]

$$\check{f}(p, \phi) = \int_{\text{path}} ds\, f(x, y), \tag{1}$$

where ds is the length element along the path of the ray assumed to be a line. Using another notation, the output wave-front distribution must be proportional to

$$\mathcal{R}_\phi\{f(\vec{x})\} \equiv \check{f}(p, \phi) = \int d\vec{x}\, f(\vec{x})\, \delta(p - \hat{\xi} \cdot \vec{x}), \tag{2}$$

where $\vec{x} = (x, y)$, $\hat{\xi} = (\cos\phi, \sin\phi)$, $p = x\cos\phi + y\sin\phi$, δ is the Dirac delta and $\mathcal{R}_\phi$ denotes the Radon transform of f at the projection angle ϕ. If two wave fronts from neighboring angular positions at angles ϕ and $\phi + \Delta\phi$ interfere, an interference pattern of the form

$$I_\phi(p) = 2\left\{1 + \cos\left[\frac{2\pi}{\lambda}\left(\check{f}(p, \phi + \Delta\phi) - \check{f}(p, \phi)\right)\right]\right\} \tag{3}$$

appears in the projection coordinate p. Interferometric techniques performed along p would then be able to give

$$\check{f}(p, \phi + \Delta\phi) - \check{f}(p, \phi) \propto \frac{d}{d\phi}\mathcal{R}_\phi\{f(\vec{x})\}. \tag{4}$$

Thus, in principle, it becomes possible to estimate experimentally the derivative of the phase projection with respect to the projection angle. That such information leads to

$\mathcal{R}_\phi\{df(\vec{x})/d\phi\}$ can be seen as follows. First, consider

$$\frac{d}{d\phi}\mathcal{R}_\phi\{f(\vec{x})\} = \int d\vec{x}\left\{f(\vec{x})\frac{d}{d\phi}\delta(p-\hat{\xi}\cdot\vec{x}) + \delta(p-\hat{\xi}\cdot\vec{x})\frac{df(\vec{x})}{d\phi}\right\}. \tag{5}$$

But

$$\frac{d}{d\phi}\delta\left(p-\hat{\xi}\cdot\vec{x}\right) = -\frac{d\delta(u)}{du}\left[\vec{x}\cdot\frac{\partial\hat{\xi}}{\partial\phi} + \hat{\xi}\cdot\frac{\partial\vec{x}}{\partial\phi}\right], \tag{6}$$

where the chain rule has been used and $u = p - \hat{\xi}\cdot\vec{x}$. The second factor of Eq. (6) turns out to be zero because along a line, $\vec{x} = (x, p/\sin\phi - x\cot\phi)$, so $\hat{\xi}\cdot(\partial\vec{x}/\partial\phi) = -(p\cos\phi/\sin\phi) + (x/\sin\phi)$. As a consequence of Eq. (5)

$$\frac{d}{d\phi}\mathcal{R}_\phi\{f(\vec{x})\} = \mathcal{R}_\phi\left\{\frac{df(\vec{x})}{d\phi}\right\}. \tag{7}$$

By invoking the Fourier-slice theorem [8, 9], if $g(\vec{x}) = df(\vec{x})/d\phi$, it follows that the Random transform $\mathcal{R}_\phi\{g(\vec{x})\}$ leads to the reconstruction of the angular derivative of $f(x,y)$ with appropriate inversion techniques. On the other side, Eq. (7) states that such a reconstruction can also be achieved with the help of usual reconstruction methods applied to $d(\mathcal{R}_\phi\{f(\vec{x})\})/d\phi$ instead of $\mathcal{R}_\phi\{df(\vec{x})/d\phi\}$. But according to Eq. (4), the former quantity can be experimentally estimated with differences of adjacent, parallel projections. So, the angular derivative of $f(x,y)$ can be reconstructed with data coming from differences of adjacent projections.

3. ANGULAR DERIVATIVE FOR A RECTANGULAR OBJECT DISTRIBUTION: AN ANALYTICAL EXAMPLE

As an example of reconstruction based on an object's angular derivative, consider first the centered rectangle of sides a, b

$$f(\vec{x}) = \mathrm{rect}\left(\frac{x}{a}\right)\mathrm{rect}\left(\frac{y}{b}\right) \tag{8}$$

as an index distribution. Thus, its derivative respect to the projection angle can be determined from the following general relation:

$$\begin{aligned}\frac{df(\vec{x})}{d\phi} &= \frac{\partial f}{\partial x}\frac{\partial x}{\partial\phi} + \frac{\partial f}{\partial y}\frac{\partial y}{\partial\phi}\\ &= -r\sin\phi\frac{\partial f}{\partial x} + r\cos\phi\frac{\partial f}{\partial y}\\ &= -y\frac{\partial f}{\partial x} + x\frac{\partial f}{\partial y},\end{aligned} \tag{9}$$

with $r^2 = x^2 + y^2$, and for the particular case of Eq. (8) (see Ref. 10, for example)

$$\frac{\partial f}{\partial x} = \left[\delta\left(x + \frac{a}{2}\right) - \delta\left(x - \frac{a}{2}\right)\right] \operatorname{rect}\left(\frac{y}{b}\right), \tag{10}$$

$$\frac{\partial f}{\partial y} = \left[\delta\left(y + \frac{b}{2}\right) - \delta\left(y - \frac{b}{2}\right)\right] \operatorname{rect}\left(\frac{x}{a}\right). \tag{11}$$

Then

$$\frac{df}{d\phi} = y\left[\delta\left(x + \frac{a}{2}\right) - \delta\left(x - \frac{a}{2}\right)\right] \operatorname{rect}\left(\frac{y}{b}\right) + x\left[\delta\left(y + \frac{b}{2}\right) - \delta\left(y - \frac{b}{2}\right)\right] \operatorname{rect}\left(\frac{x}{a}\right), \tag{12}$$

and a plot is drawn in Fig. 1a. The borders of the phase distribution are indicated by Dirac delta impulses. The heigh of the impulses shows a linear modulation. This linear modulation is quite general and can be seen as a consequence of Eq. (9). If the rectangle is decentered to $(a/2, b/2)$, it can be shown that

$$\frac{df}{d\phi} = y[\delta(x) - \delta(x - a)] \operatorname{rect}\left(\frac{y - b/2}{b}\right) + x[\delta(y) - \delta(y - b)] \operatorname{rect}\left(\frac{x - a/2}{a}\right), \tag{13}$$

whose plot is to be seen at Fig. 1b. The enhancement of the rectangle's edges due to modulated Dirac delta impulses shows its zero values at different relative locations as in the centered case. The impulse values can be higher as in the centered case, which means more sensitivity in detection.

4. RECONSTRUCTION OF PARALLEL PROJECTIONS DIFFERENCES: NUMERICAL EXAMPLES

4.1. UNIT SQUARE

The parallel projections of a unit square were calculated in order to carry out its reconstruction with a backprojection algorithm [11] (backprojection grid of 65×65 pixels, a reconstruction is shown in Fig. 1c). Differences between adjacent projections were also calculated and then subject to the same backprojection algorithm. For the calculations the relation $f(x, y) = n_0[1 - \beta(x, y)]$ was employed, where n_0 denotes the average refractive index and $\beta(x, y)$ the refractive index variations in fractions of n_0. The values shown in subsequent graphs comes from

$$\frac{f(x, y)}{n_0}, \tag{14}$$

n_0 remaining undetermined. Figure 1d shows the three-dimensional reconstruction of a centered square's projection differences retrieved with a backprojection algorithm (992

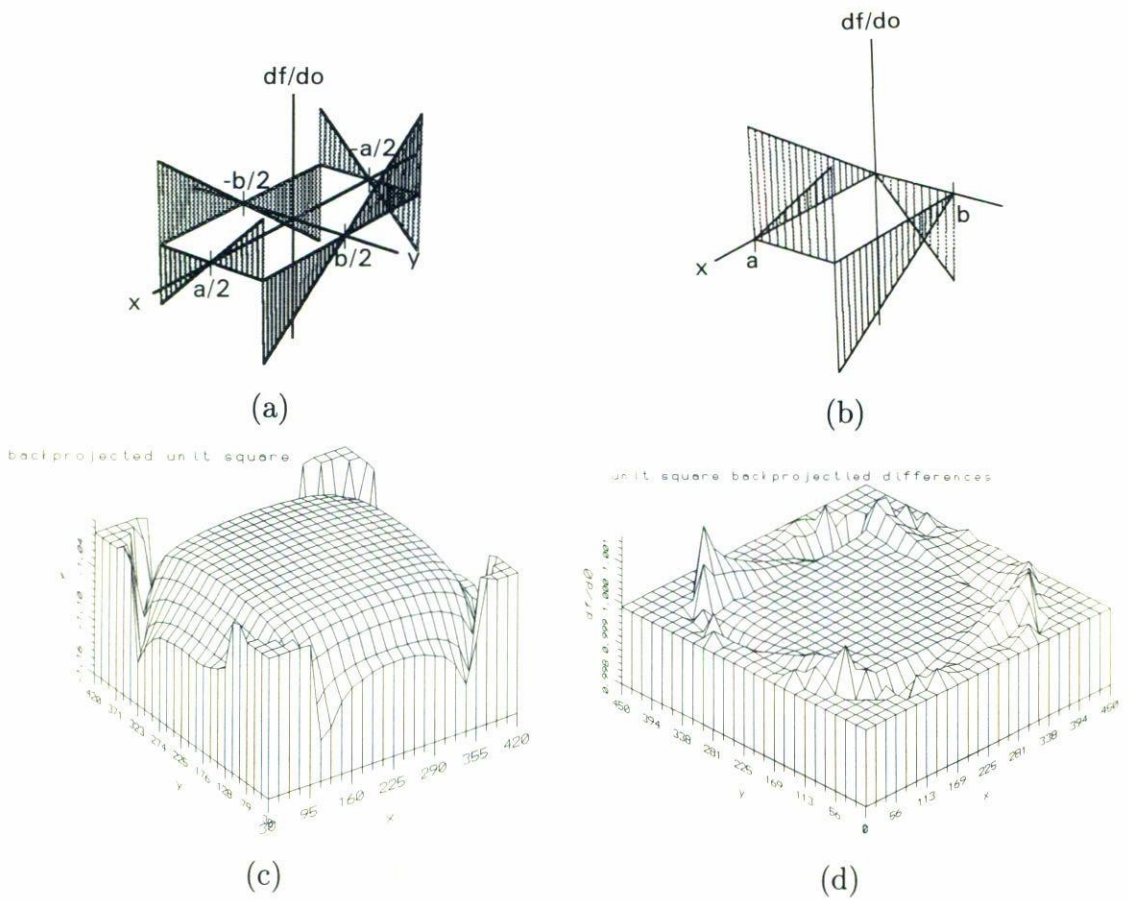

FIGURE 1. Angular derivatives of a rectangle with sides a, b (a) centered, (b) translated along $(a/2, b/2)$, (c) reconstruction of unit square (seen from below), (d) three-dimensional reconstruction of the unit square's parallel projection differences: the same backprojection algorithm was used for (c) and (d).

projections, $\Delta\phi = 0.363°$). The effect of edge enhancement and linear modulation can be recognized to be in agreement with the derivative depicted in Fig. 1a for the case $a = b = 1$. The implemented algorithm introduces a factor of roughly 0.1 in the refractive-index values, so the units on the z-axis are arbitrary.

4.2. CENTERED ELLIPSES

Figure 2 shows the reconstruction of two objects (left column) and the corresponding backprojected projection differences (right column) using the same algorithm for all cases. The axis labels of the gray-level plots denote the pixel number rather than the positions. Then, the position coordinate origin must be located at the pixel coordinates $(33, 33)$. At the upper row (left) it is shown an object reconstructed with the addition of parallel projections calculated for two centered ellipses with axis parallel to the coordinate ones.

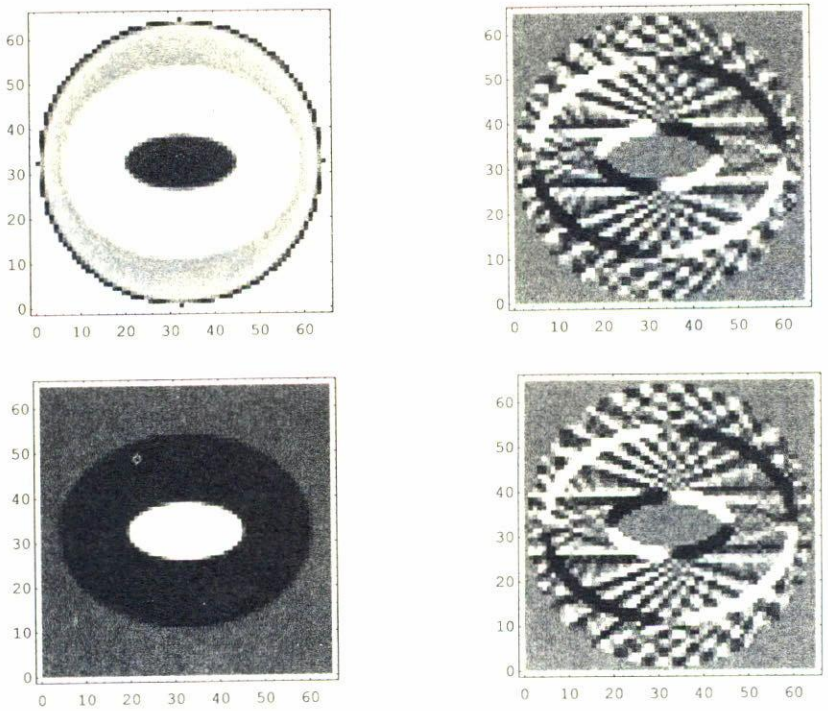

FIGURE 2. Density plots of reconstruction of objects (column at left) and corresponding differences (column at right). Upper row: addition of two centered ellipses. Lower row: subtraction of the same pair.

Each ellipse has a constant value of refractive index (β-values of 0.3 and 0.7). The lower row (left) shows the reconstruction of another object made by subtracting the same parallel projections of the two ellipses of the previous case. In both cases the number of projections was 180 and, for the differences of projections, the value $\Delta\phi = 2°$ was employed. Because the differences tend to adopt lower values, the noise appears to be comparable with the signal. Thus, typical backprojection artifacts begin to be noticeable. Note at the right column that the values of the linear modulation of the inner ellipse's edge go either above (bright) or below (dark) the background level (gray) according to the sign of its index with respect to the outer ellipse's index: for the case of ellipse addition, the bright and dark edge irradiance are found at the same quadrants. In contrast, for the case of ellipse subtraction, opposite irradiance levels are found in the same quadrant. Therefore, this effect gives a hint of the gradient's sign of the phase distribution.

4.3. ROTATED, DESCENTERED ELLIPSES

Figure 3 shows a reconstructed phase "phantom head" (left column) made of translated and rotated ellipses, each of a constant refractive index. The following values of β and rotation angles (major axis respect to the horizontal axis) for each of the four ellipses were used: 0.7 (72°), 0.7 (108°), 0.95 (90°), and 0.25 (90°, bigger ellipse.) Backprojection of corresponding projection differences are to be seen at the right column. The lower

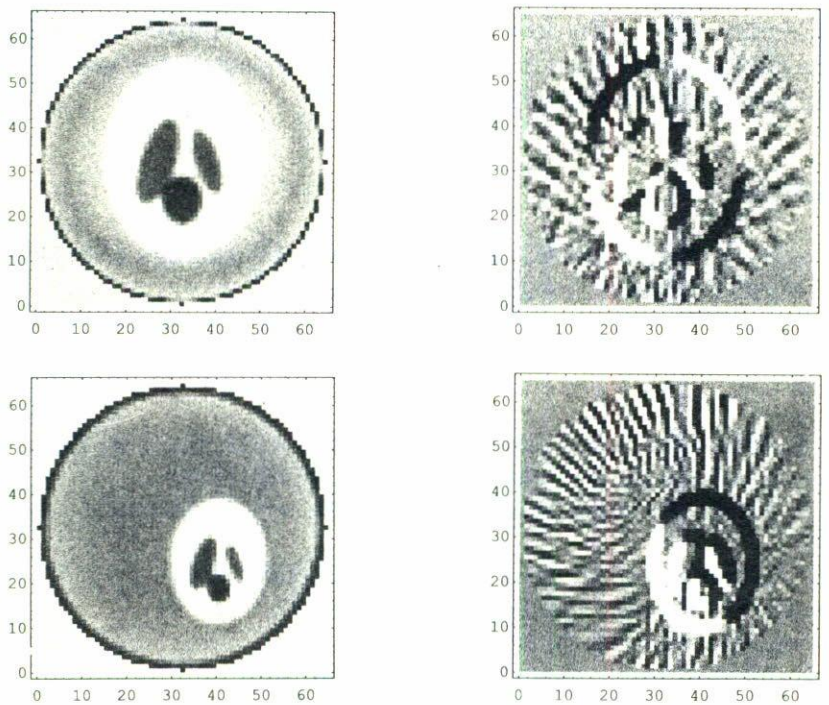

FIGURE 3. Density plots of reconstruction of "phantom heads" (column at left) and corresponding differences (column at right). Upper row: centered phantom. Lower row: translated phantom.

row displays the same phantom as in the upper row, but translated as a whole from the origin of the position coordinate to show its respective modulation depth (as refereed in Fig. 1b). As compared with the first case, the resulting dark and bright irradiance distribution is found in halves and not in quadrants, it departs from the background level in a more appreciable way (*i.e.*, along a higher proportion of the whole edge), and it is thicker.

5. FINAL COMMENTS

A relation between the Radon transform of a function defined in two dimensions and its angular derivative was deduced and employed to propose a new technique of potential use in tomography. The proposed method leads to the enhancement of refractive-index gradients with no circular symmetry respect to the rotation axis [$\check{f}(p, \phi + \Delta\phi) = \check{f}(p, \phi)$ results in a derivative with value of zero]. Objects with circular symmetry can be adapted for the technique just translating the object so as to breake such symmetry. Numerical simulations confirm its suitability for optical tomography. Such a method does not need of an integration process for edge detection and can be carried out iteratively with the appropriate dynamic recording media (photorefractive crystals, for example). The effect described resembles the well known edge-enhancement effect (image differentiation) by optical spatial filtering carried out with a filter having linear amplitude absorption along

some fixed direction [12]. The low values of the phase differences demand of phase measurements having good signal-to-noise ratio, which suggest the use of heterodyne or phase-shifting interferometric measurements.

ACKNOWLEDGMENTS

The authors want to thank CONACyT for partial support through code 3649E. Valuable help from E. Marti-Panameño are greatly appreciated.

REFERENCES

1. X. Wang, R. Magnusson, and A. Haji-Sheikh, *Appl. Opt.* **32**, 11 (1993) 1983.
2. D. Dirksen and G. von Bally, *J. Opt. Soc. Am.* **11**, 9 (1994) 1858.
3. T. Sato, T. Susuki, P.J. Bryanston-Cross, O. Ikeda, and T. Hatsuzawa, *Appl. Opt.* **22**, 6 (1983) 815.
4. T. Sato, T. Hatsuzawa and O. Ikeda, *Appl. Opt.* **22**, (1983) 3895.
5. R. Snyder and L. Hesselink, *Opt. Lett.* **13**, 12 (1988) 87.
6. D. Verhoeven, *Appl. Opt.* **32**, 20 (1993) 3736.
7. G.W. Faris and H.M. Hertz, *Appl. Opt.* **28**, 21 (1989) 4662.
8. S.R. Deans, *The radon transform and some of its applications* (John Wiley and Sons, 1983).
9. A.C. Kak and M. Slaney, *Principles of computerized tomographic imaging* (IEEE Press, 1987).
10. R.N. Bracewell, *The Fourier transform and its applications* (McGraw-Hill, 1978).
11. J. Soto, *Appl. Opt.* **32**, 35 (1994) 7272.
12. R.S. Sirohi and V. Ram Mohan, *Optica Acta* **24**, 11 (1977) 1105.